

# PMMA Microcapsules for the Inactivation of SARS-CoV-2

Vânia I. Sousa, Joana F. Parente, Juliana F. Marques, Carla Calçada, Maria I. Veiga, Nuno S. Osório, and Carlos J. Tavares\*



Cite This: *ACS Omega* 2022, 7, 22383–22393



Read Online

ACCESS |

Metrics & More

Article Recommendations

**ABSTRACT:** Surface disinfection currently plays a decisive role in the epidemiological situation caused by the SARS-CoV-2 coronavirus. However, most disinfection products available on the market have a high evaporation rate and only an immediate action and not continuous, creating the need for a high frequency of disinfection. To overcome this limitation, in the present work, poly(methyl methacrylate) (PMMA) microcapsules were developed with an active agent (hydrogen peroxide) encapsulated, which has the ability to inactivate/neutralize the SARS-CoV-2 virus. PMMA-H<sub>2</sub>O<sub>2</sub> microcapsules have a spherical shape and a smooth structure with low porosity and were successfully attached to nonwoven fabrics, as observed from scanning electron microscopy. The thermogravimetric analysis shows that PMMA-H<sub>2</sub>O<sub>2</sub> microcapsules have high thermal stability and can increase the stability of H<sub>2</sub>O<sub>2</sub>. Nonfabric substrates functionalized with PMMA-H<sub>2</sub>O<sub>2</sub> microcapsules were tested by a highly sensitive and specific reverse transcription-quantitative real-time polymerase chain reaction (RT-qPCR)-based method to evaluate antiviral activity through the degradation of SARS-CoV-2 deoxyribonucleic acids. The highest percentage of viral nucleic acid elimination was obtained when exposing the viral sample for 1 h to PMMA-H<sub>2</sub>O<sub>2</sub> microcapsules, resulting in an elimination of >97% of the coronavirus. In addition, the microcapsules are stable over a period of three weeks and retain the ability to eliminate SARS-CoV-2. Hence, it is demonstrated that this microcapsule system is efficient for SARS-CoV-2 elimination and inherent surface disinfection.



## 1. INTRODUCTION

The emergence of SARS-CoV-2 virus has become a serious threat to public health.<sup>1</sup> Since the end of 2019, the world has been trying to control the pandemic outbreak caused by COVID-19 disease, which as of September 14, 2021, had caused 4,547,782 deaths in 219,456,675 cases of infection.<sup>2</sup> Identified in 1960, coronaviruses are a family of viruses that naturally reside in animals, mainly in some species of bats.<sup>3</sup> When present in humans, it can cause respiratory illnesses, from constipation to pneumonia.<sup>4</sup> In early December 2019, in the city of Wuhan (Hubei Province, China), pneumonia of unknown etiology was diagnosed in several patients.<sup>5</sup>

On the 31st of the same month, the Wuhan Municipal Health Commission reported to the World Health Organization (WHO) 27 cases of pneumonia of unknown cause.<sup>6</sup> Most of the patients worked or lived in the local wholesale market in Huanan Seafood, where live animals were also traded. On January 7, 2020, a new coronavirus was identified (2019-nCoV), having >95% homology to the bat coronavirus and >70% similarity to SARS-CoV.<sup>5</sup> This new virus was later renamed severe acute respiratory syndrome coronavirus 2 (SARS-CoV-2) by the Coronavirus Study Group and the associated disease was named coronavirus 2019 disease (COVID-19) by the WHO. The number of cases increased

exponentially, with several cases occurring where there was no exposure to the live animal market, which suggested the occurrence of transmission between humans.<sup>7</sup> Although there is still not enough information about the exact form of transmission between humans, it is suggested that SARS-CoV-2 is transmitted through the airway, through aerosol droplets expelled from the nose and mouth.<sup>8</sup> These respiratory droplets can remain on surfaces and objects for several minutes or several days, depending on the type of material.<sup>9</sup> Infectiousness stability is greater on smooth surfaces such as glass, wood, and stainless steel.<sup>9</sup> Adsorption of SARS-CoV-2 on everyday surfaces causes high technological, medical, and public health constraints. Therefore, frequent surface disinfection plays a key role in controlling COVID-19.<sup>10</sup> Several conventional disinfectants are active against the SARS-CoV-2 virus, and the most frequently used ones are bleach, hydrogen peroxide, and alcohol solutions.<sup>11</sup> These products available on the

Received: March 10, 2022

Accepted: June 7, 2022

Published: June 22, 2022



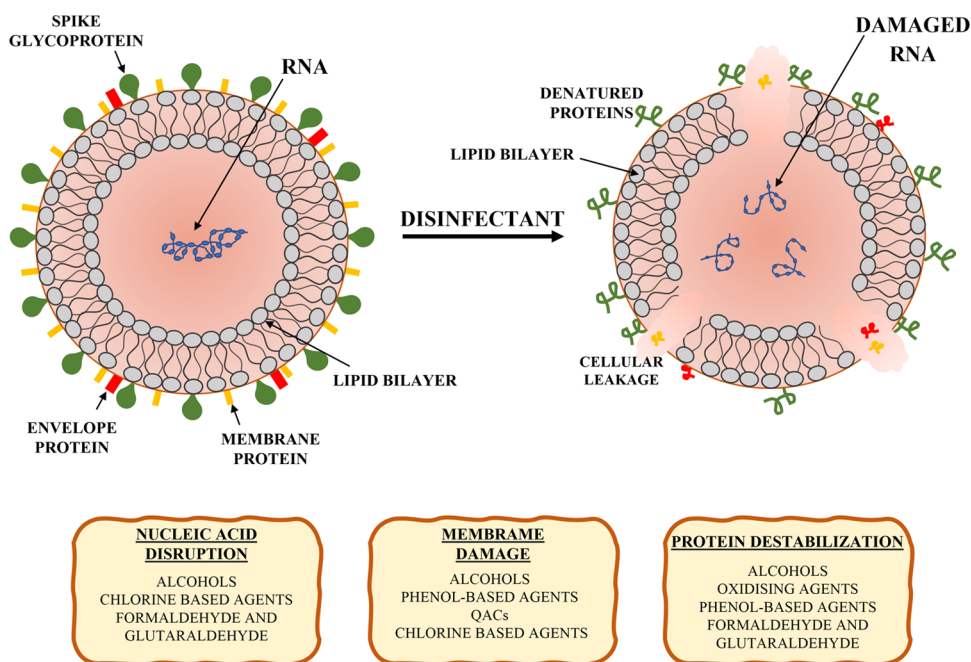


**Figure 1.** Structural components of SARS-CoV-2 (left) and action of effective biocidal agents to inactivate the virus (right) (adapted with permission from ROWAN, N. J.; MEADE, E.; GARVEY, M. EFFICACY OF FRONTLINE CHEMICAL BIOCIDES AND DISINFECTION APPROACHES FOR INACTIVATING SARS-COV-2 VARIANTS OF CONCERN THAT CAUSE CORONAVIRUS DISEASE WITH THE EMERGENCE OF OPPORTUNITIES FOR GREEN ECO-SOLUTIONS. CURR. OPIN. ENVIRON. SCI. HEAL. 2021, 23, 100290. 2021 ELSEVIER).

market are effective in a very short space of time due to their high rate of evaporation, corrosivity, and immediate action, implying frequent applications on surfaces to be disinfected.<sup>1</sup> Due to this fact, there is a market need to develop new materials that maximize the action of these disinfecting agents to prolong the sterilization time and reduce the need and frequency of their application by the end-user. Micro-encapsulation appears as an alternative to overcome this limitation. This methodology is able to provide stability to the active agents of disinfectants, allowing the safe transport of this type of substance, which is normally highly volatile. Furthermore, the encapsulation allows controlled release, for example by mechanical action when walking on a floor that has been cleaned with a disinfectant product with encapsulated active agents.<sup>12</sup>

Like sodium hypochlorite and ethyl alcohol, hydrogen peroxide is also commonly used in disinfectant products.  $H_2O_2$  is an oxygen-producing chemical, as it breaks down into water and oxygen.<sup>13</sup> Although there are several studies that report the encapsulation of oils through different techniques,<sup>14–17</sup> the synthesis of microcapsules (MCs) filled with aqueous compounds is underexplored and historically difficult, especially with liquids that are extremely hydrophilic.<sup>18</sup> This product is bactericidal, sporicidal, and fungicidal and has the ability to inactivate viruses including SARS-CoV-2. It acts by attacking the lipid membrane, deoxyribonucleic acid, and other components essential to the cell's life (Figure 1).<sup>19,20</sup>

Only a few studies have reported the microencapsulation of  $H_2O_2$  in polymeric matrices, and none of these studies aimed to use this chemical as a disinfectant and virus inactivator.<sup>21–23</sup> The microencapsulation of  $H_2O_2$  in poly(methyl methacrylate) PMMA matrix has already been reported, but the application of this polymeric system in disinfection has not yet been evaluated.<sup>23</sup> In this article, the evaluation of antiviral activity is

carried out through the degradation of SARS-CoV-2 deoxyribonucleic acids. These microcapsules have the potential for direct applications in disinfectant products that can be applied in textile material to provide properties such as self-cleaning surfaces and/or antimicrobial resistance. Application on nonwoven fabrics is performed in this article and their efficiency tested. Nonwoven textiles have random fiber conformation, filtration capacity, permeability, and porosity, resulting in their frequent use in medicinal environments.<sup>24</sup>

This work reports the development of a microcapsule system with an encapsulated active disinfectant agent capable of immobilizing and/or neutralizing the SARS-CoV-2 virus on various surfaces, such as fabrics (e.g., masks, gloves, clothing, seats for private and public transport vehicles), metals (e.g., elevators, door handles, railings, and handrails), plastics (e.g., switches, kitchen utensils), walls, and floors. Through the impregnation of these intelligent materials on different surfaces, it will be possible to increase the time and effectiveness of the action of the disinfectant agents, decrease the viral presence on frequently touched surfaces and maintain them virus-free for longer periods.

## 2. EXPERIMENTAL DETAILS

**2.1. Materials.** Polymethylmethacrylate (PMMA) with a weight average ( $M_w$ ) of 550,000 g/mol (based on GPC analysis) and poly(vinyl alcohol) (PVA, 98–99%) were purchased from Alfa Aesar (Massachusetts, EUA) and used as received. Chloroform was purchased from LabChem (Pennsylvania). An anionic surfactant, sodium dodecyl sulfate (SDS), was provided by Acros Organics (New Jersey). Hydrogen peroxide (30 wt %) in a water solution was purchased from Scharlab (Barcelona, Spain). The BAYPRET NANO-PU solution (TANATEX Chemicals) was used as the

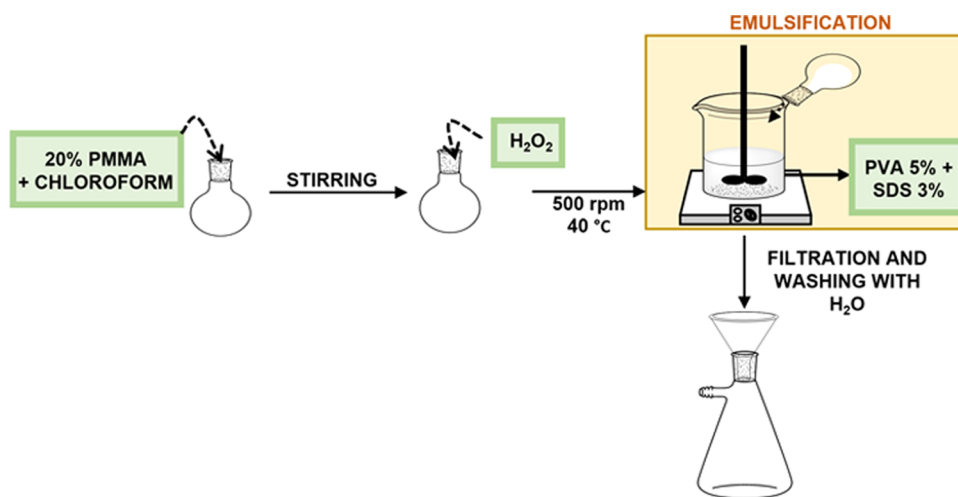


Figure 2. Representative scheme of the synthesis of PMMA-H<sub>2</sub>O<sub>2</sub> microcapsules.

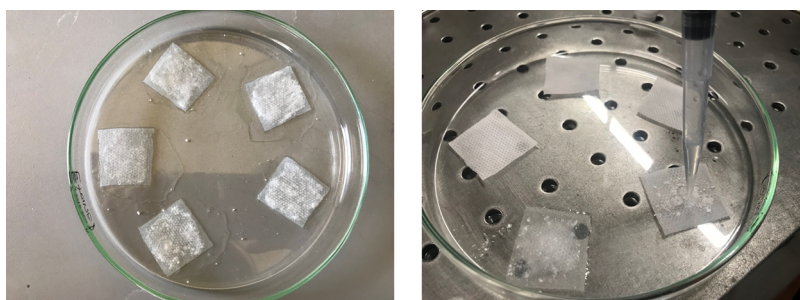


Figure 3. Photographic records of the preparation of nonwoven fabric samples with PMMA-H<sub>2</sub>O<sub>2</sub> MCs.

subtract binder. All chemicals were used as supplied without further treatment.

**2.2. Microcapsule Synthesis.** The PMMA microcapsules (MCs) were synthesized by a solvent evaporation method (Figure 2), where an oil-in-water (o/w) emulsion is created using a mechanical stirrer. In the first stage, the polymer was dissolved in chloroform under magnetic stirring for at least 24 h at ambient temperature to form an oil phase. The active agent (H<sub>2</sub>O<sub>2</sub>) was then added to the above-mentioned solution and the system was magnetically stirred for a further 10 min. In the second stage, the solution was added dropwise to an aqueous solution of 3 wt % SDS and 5 wt % PVA, under mechanical mixing at 500 rpm (IKA, model EUROSTAR 20) at 40 °C. The solution was allowed to stir until the evaporation of the solvent was complete (1 h). The resulting microcapsules were rinsed several times with water to remove any unreacted reagent.

**2.3. Morphological, Thermal, and Structural Characterizations.** The surface and morphology of microcapsules were observed in an ultrahigh-resolution field emission gun scanning electron microscope (FEG-SEM), NOVA 200 Nano SEM, FEI Company, at SEMAT/UM, University of Minho. Topographic images were obtained with a secondary electron detector at an acceleration voltage of 10 kV. Before morphological analysis, PMMA-H<sub>2</sub>O<sub>2</sub> microcapsules were covered with a thin film (50 nm) of Au-Pd (80–20 wt %), with a high-resolution sputter coater, 208HR Cressington Company, coupled to an MTM-20 Cressington high-resolution thickness controller. Thermal analysis of PMMA-H<sub>2</sub>O<sub>2</sub> microcapsules was conducted on a Hitachi STA 7200 simultaneous thermal analyzer (Japan). Each experiment was conducted with

a sample weight ranging from 9 to 12 mg and placed in 5 mm diameter aluminum pans. The latter experiments were performed under a nitrogen atmosphere with a flow rate of 250 mL/min. In the dynamic analysis, the samples were heated from 30 to 600 °C at a constant rate of 10 °C/min. The mass change was recorded throughout the experiment. Thermal analyses were performed in triplicate.

To study the chemical structure of microcapsules, attenuated total reflectance-Fourier transform infrared (ATR-FTIR) spectra were recorded using a Spectrum 2 FTIR spectrophotometer (ATR-FTIR, Perkin Elmer, Waltham, MA). The ATR-FTIR spectrum was recorded over the range of 4000–450 cm<sup>-1</sup>, with a resolution of 4 cm<sup>-1</sup>. The spectra were collected in transmittance mode on a pure diamond ATR crystal cell by the accumulation of four scans.

**2.4. SARS-CoV-2 Deoxyribonucleic Acid Degradation Assay.** Nonwoven fabrics were chosen as substrates to perform the antiviral activity tests to evaluate the efficacy of PMMA-H<sub>2</sub>O<sub>2</sub> MCs in SARS-CoV-2 virus inactivation. Synthesized PMMA-H<sub>2</sub>O<sub>2</sub> MCs were dispersed into an aqueous solution of the textile binder BAYPRET NANO-PU. The resultant suspension was then loaded onto nonwoven fabric samples (1 cm × 1 cm), covering the entire substrate area (Figure 3). The functionalized samples were dried for 4 h at 40 °C. Nonwoven fabric samples were prepared with PMMA-H<sub>2</sub>O<sub>2</sub> MCs of three different concentrations, 12.5, 25, and 50 mg/cm<sup>2</sup>.

A previously developed<sup>25</sup> highly sensitive SARS-CoV-2 ribonucleic acid degradation assay was performed to measure the antiviral activity of the PMMA-H<sub>2</sub>O<sub>2</sub> microcapsules. In this assay, the exposure experiments were completed from a fresh

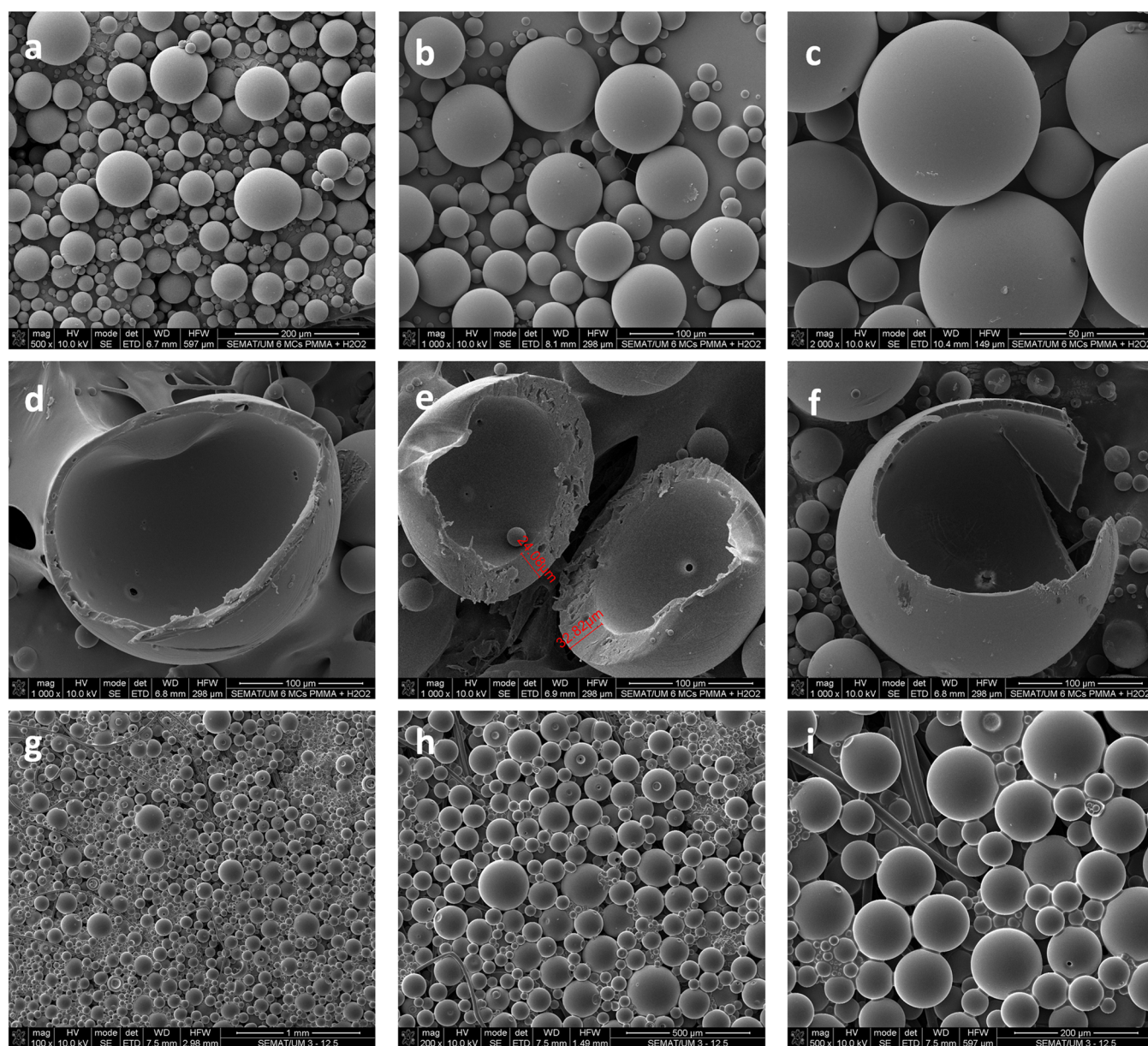


**Figure 4.** SEM micrographs of PMMA-H<sub>2</sub>O<sub>2</sub> MCs with magnifications of (a) 500×, (b) 1,000×, and (c) 2,000×. (d)–(f) Shell thickness of PMMA-H<sub>2</sub>O<sub>2</sub> MCs with the magnification of 100×; nonwoven fabric samples with PMMA-H<sub>2</sub>O<sub>2</sub> MCs with magnifications of (g) 100×, (h) 200×, and (i) 500×.

swab clinical sample, before nucleic acid extraction and the synthesis of cDNA, to evaluate the degradation of SARS-CoV-2 deoxyribonucleic acids as detailed elsewhere.<sup>26</sup> SARS-CoV-2 samples derived from excess swab samples diagnosed through RT-qPCR as SARS-CoV-2 positive at the diagnostic laboratory from ICVS, University of Minho. Experiments with SARS-CoV-2 isolates derived from human nasal swabs were approved by the competent Institutional Review Board, Comissão de Ética para a Investigação em Ciências da Vida e da Saúde (CEICVS), with the reference CEICVS008/2022. For this assay, fresh swab samples were diluted to contain approximately 1000–3000 viral copies per mL considering the quantification cycle (C<sub>q</sub>) of the RT-qPCR assay in relation to the commercial standard reference, EDX SARS-CoV-2 Standard (SKU: COV019, BioRad) containing synthetic RNA transcripts of SARS-CoV-2 E, N, ORF1ab, RdRP, and S genes, at 200,000 copies/mL.

Samples of 1 cm<sup>2</sup> square of nonfabric substrates, with and without functionalization with PMMA or PMMA-H<sub>2</sub>O<sub>2</sub>, were inoculated with 60 μL of the swab sample placed in the center of the tissue square. The exposure was done at different times (10, 30, or 60 min). The procedure was performed inside a negative pressure laboratory and using a flow chamber cabinet by trained BSL3 operators. After viral exposure, sample inactivation was done by adding 250 μL of lysis buffer, vortexing vigorously for 30 s, and incubating at 56 °C for 10 min. RNA was then extracted following the NZY Viral RNA isolation kit, MB40701 (2020 NZYTech, Lda, Portugal) according to the manufacturer's instructions. The RT-qPCR reactions were performed using the OmniSARS2 assay.<sup>25</sup> Briefly, the assay detects three different SARS-CoV-2 genes (ORF1ab, S, and E) and the human RNP gene as an internal control. Reactions were set for a final volume of 30 μL reaction, containing 10 μL of RNA sample and the remaining

volume of NZYSupreme One-Step RT-qPCR Probe Master Mix, MB414 (2020 NZYTech, Lda, Lisbon, Portugal) and the oligonucleotides at a final concentration of 333 nM each SARS-CoV-2 primer, 84 nM each SARS-CoV-2 probe, 267 nM internal control primer, and 67 nM internal control probe. The reactions were incubated at 50 °C for 20 min (reverse transcription), followed by incubation at 95 °C for 2 min (inactivation reverse transcriptase/polymerase activation) and 45 cycles of 95 °C for 5 s (denaturation) and 60 °C for 30 s (annealing/extension with the signal acquisition). RT-qPCR assays were performed on QuantStudio 6 Pro (Applied Biosystem by Thermo Fisher Scientific) and analyzed by Design & Analysis Software, version 2.4.3 (2020 Thermo Fisher Scientific), including linear regression and absolute quantification analysis. Viral load in the tested samples was calculated using absolute quantification from the Cq standard curve of each viral probe determined with the commercial standard reference, EDX SARS-CoV-2 Standard (SKU: COV019, BioRad, Hercules, CA).<sup>25</sup> Assays performed in nonfabric substrates, with and without functionalization with PMMA or PMMA-H<sub>2</sub>O<sub>2</sub>, were done at least in triplicate, with more tests being carried out under more relevant conditions, to ensure reproducibility. The percentage of viral elimination was calculated using Cq values and respective viral quantification load obtained from the control samples (nonfunctionalized fabric) minus the viral load obtained in the functionalized fabric. The percentage of viral elimination was calculated using the following equation

$$\text{viral elimination(\%)} = \frac{[\text{exposed copies}(\text{mL}^{-1}) - \text{control copies}(\text{mL}^{-1})]}{\text{control copies}(\text{mL}^{-1})} \times 100 \quad (1)$$

### 3. RESULTS AND DISCUSSION

**3.1. Microcapsule Morphology.** The control of the PMMA MCs morphology is essential for attaining the desired properties according to their final application. Furthermore, the morphology is highly dependent on the choice of polymers that hold the core material and the parameters used in the synthesis.

As shown in the SEM micrographs in Figure 4, the PMMA MCs (without the active agent) in Figure 4a–c and the PMMA-H<sub>2</sub>O<sub>2</sub> MCs in Figure 4d–f have a regular spherical shape with a smooth, sealed, and pore-free structure. In all SEM micrographs, no significant aggregation is seen. Figure 4g–i shows the surface morphology of fabric samples with impregnation of PMMA-H<sub>2</sub>O<sub>2</sub> MCs. It is possible to observe that the dispersion of microcapsules in the fabric is feasible, although there is some agglomeration of the microcapsules, which is probably caused by the BAYPRET NANO-PU during the impregnation process. However, it is apparent that the microcapsules are efficiently attached to the surface of the nonwoven fabric.

The heterogeneity in the size of both microcapsule systems is verified. The heterogeneity of the size distribution is probably caused by the stirring process during the synthesis. The agglomeration of the oil phase potentiates the formation of microcapsules of inhomogeneous size. Furthermore, as the water–oil emulsion is formed quickly around the stirrer, the smallest microcapsules are formed near the stirrer and the

larger ones further away.<sup>27</sup> PMMA MCs have an average diameter of 20 μm, within a range of 2–80 μm (Figure 5). The microcapsule wall thickness varies between 7 and 32 μm (Figure 4d–f).

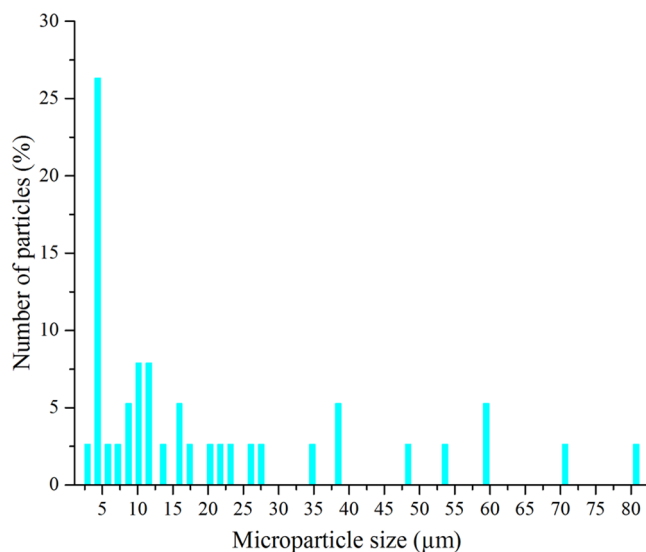


Figure 5. Particle size distribution of PMMA-H<sub>2</sub>O<sub>2</sub> microcapsules.

**3.2. Molecular Structure of Microcapsules.** The chemical structures of PMMA and PMMA microcapsules were investigated using FTIR-ATR spectroscopy. Figure 6 shows the transmittance spectra of the characteristic peaks of PMMA raw material, PMMA, and PMMA-H<sub>2</sub>O<sub>2</sub> microcapsules.

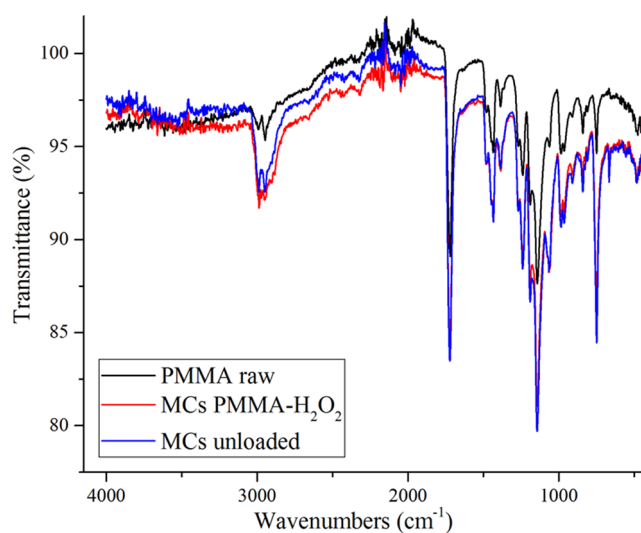
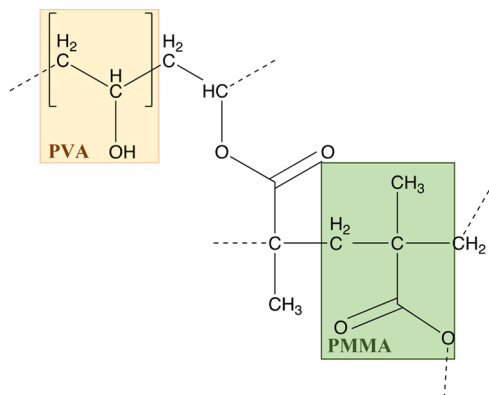


Figure 6. FTIR spectra of PMMA raw (black), PMMA microcapsules loaded with H<sub>2</sub>O<sub>2</sub> (red), and PMMA microcapsules unloaded (blue).

The absorption peak at 1720 cm<sup>-1</sup> is attributed to C=O stretching vibration. Another strong C=O peak can be seen at 748 cm<sup>-1</sup>.<sup>28</sup> The FTIR band at 1143 cm<sup>-1</sup> is assigned to the stretching vibration for C–O and the band at 1239 cm<sup>-1</sup> corresponds to the ester group and the C–O–C single bond vibration in the polymer.<sup>29</sup> The absorption peaks at 2988 and 2948 cm<sup>-1</sup> indicate the asymmetric and symmetric stretching vibrations of the C–H band in PMMA, respectively.<sup>30</sup> The

1435  $\text{cm}^{-1}$  band is assigned to the bending vibration of  $\text{CH}_3$ .<sup>31</sup> FTIR spectra of PMMA raw material and loaded and unloaded PMMA MCs are identical, except for the presence of a peak at 667  $\text{cm}^{-1}$  in the MC spectrum. The absence of the peak in the raw material spectrum may indicate a possible change in the chemical structure of the polymer during the synthesis of microcapsules. PMMA may have reacted with PVA (Figure 7)



**Figure 7.** Possible polymerization reaction between poly(methyl methacrylate) and poly(vinyl alcohol).

to form C–O bonds that could present a vibrational band at 667  $\text{cm}^{-1}$ .<sup>32</sup> Similar FTIR results are reported for microcapsules with and without  $\text{H}_2\text{O}_2$ . This similarity of spectra may indicate that hydrogen peroxide is efficiently encapsulated and not present on the walls of the microcapsule. The results suggest that the microcapsule formation reaction that occurs does not produce changes in functional groups, since the characteristic bands remain the same.

**3.3. Thermogravimetry Analyses.** Figure 8 shows the thermogravimetric analysis (TGA) for the PMMA raw polymer, unloaded PMMA microcapsules, and PMMA microcapsules loaded with  $\text{H}_2\text{O}_2$  as a core agent. Derivative thermogravimetry (DTG) curves are presented in Figure 9. DTG curves suggest that PMMA has two main degradation

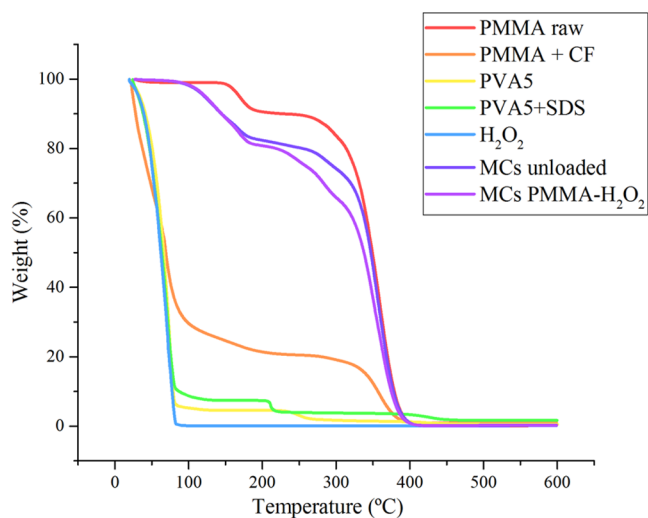


**Figure 8.** TGA curves for pure PMMA (red), PMMA + CF (orange), PVA 5% (yellow), PVA 5% + SDS (green),  $\text{H}_2\text{O}_2$  (blue), PMMA MCs (violet), and PMMA- $\text{H}_2\text{O}_2$  MCs (purple).

states, while the different MCs formed by this polymer seem to have more degradation states that are partially overlapping.

The decomposition temperature for pure PMMA and the synthesized microcapsule systems is presented in Table 1. TGA results reveal that MCs have a lower thermal resistance when compared to pure PMMA. The first degradation step, which takes place between 95 and 195  $^{\circ}\text{C}$ , is more complex for microencapsulation systems compared to pure PMMA. This complexity may result from the overlap of PMMA with the other constituents of the microcapsule, such as PVA and SDS. PMMA MCs with  $\text{H}_2\text{O}_2$  have a lower thermal resistance than unloaded microcapsules from the second stage of degradation, reaching 350  $^{\circ}\text{C}$  with a greater mass loss (62.5%).

Derivative thermogravimetry (DTG) indicates that the degradation process around 137  $^{\circ}\text{C}$  is only present in MC DTG. This degradation may be related to a synthesis reaction product between PMMA and other constituents (PVA or SDS). PMMA microcapsules loaded with  $\text{H}_2\text{O}_2$  show a degradation state at a temperature of 284  $^{\circ}\text{C}$  (peak marked with an asterisk in Figure 9) that does not occur in unloaded PMMA microcapsules, which can be related to the degradation of  $\text{H}_2\text{O}_2$ .

In general, available scientific studies<sup>33,34</sup> suggest that the depolymerization of PMMA-H occurs in the last stage of degradation, while the breaking of weaker bonds such as PMMA-HH (breaking of the HH bond of MMA oligomers) and breaking of the unsaturated ends of  $\text{CH}=\text{CH}_2$  are more likely to occur in the earlier stages.

**3.4. Antiviral Activity of PMMA MCs.** Fabric substrates functionalized with PMMA MCs with or without  $\text{H}_2\text{O}_2$  were tested for antiviral activity by evaluating the percentage of SARS-CoV-2 deoxyribonucleic acid degradation. The tests targeted three different genes of the SARS-CoV-2 genome. The exposure of SARS-CoV-2 positive samples with viral loads from 1000 to 3000 copies per mL to the fabric functionalized with PMMA resulted in the elimination of 62.27% (median) of the viruses after 10 min (Figure 10). Increasing the time of exposure to 30 min or 1 h resulted in an increase in the percentage of SARS-CoV-2 elimination to values above 75% (Figure 10). The highest percentage of viral elimination was obtained when the viral sample was exposed to PMMA- $\text{H}_2\text{O}_2$  MCs for 1 h (Figure 10). This condition resulted in the reduction by 97.26% (median) of the virus deoxyribonucleic acid and consequently its elimination.

The highly efficient rate of viral elimination obtained by exposure to PMMA- $\text{H}_2\text{O}_2$  MCs was found to be dependent on the presence of microcapsules since the direct exposure of the components present in the MC formulation has a significantly lower effect on the detection of the virus (Figure 11). The nonwoven fabric, solvent, polymer base, and binder have an irrelevant effect on virus detection (less than 15% in samples tested). An analysis of surfactants and empty MCs showed that 45.67 and 20.54% of them have been eliminated, respectively. These results can be explained by the ability of surfactants, such as SDS and PVA, to reduce the incidence of infectivity of several viruses. These surfactants can interact with SARS-CoV-2, dissolving their lipid bilayer and promoting the total disruption of the virus, leading to its inactivation. In empty MCs, the effect is not as pronounced when compared to surfactants because their amount becomes residual after the microcapsule synthesis. When microcapsules are loaded with  $\text{H}_2\text{O}_2$  at three different concentration levels ( $c_1 = 12.5 \text{ mg}/\text{cm}^2$ ,  $c_2 = 25 \text{ mg}/\text{cm}^2$ , and  $c_3 = 50 \text{ mg}/\text{cm}^2$ ), it is possible to

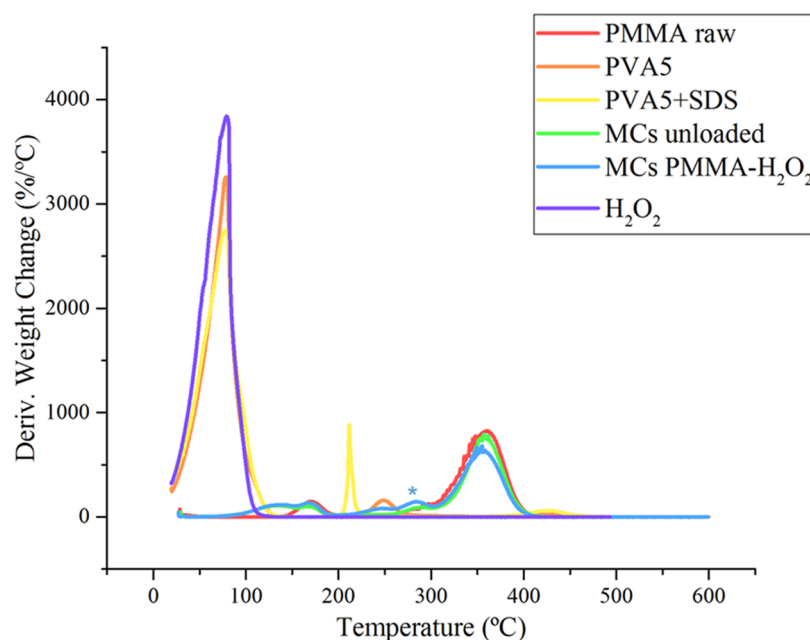


**Figure 9.** DTG curves for pure PMMA (red), PVA 5% (orange), PVA 5% + SDS (yellow), PMMA MCs (green), PMMA-H<sub>2</sub>O<sub>2</sub> MCs (blue), and H<sub>2</sub>O<sub>2</sub> (violet).

**Table 1.** Solvent Evaporation Temperature (5% wt Loss), Temperature, and Percentage of wt Loss for Degradation Steps and Percentage of Residual Material at 350 °C for Pure PMMA and PMMA MC Systems

samples	5% wt loss (°C)	1st degradation step (°C/% wt loss)	2nd/3rd degradation Step (°C/% wt loss)	residual material at 350 °C (% wt loss)
PMMA	168.4	140–195/98.2–90.7	260–420/89.3–0.06	48.2
PMMA MCs	121.2	95–195/98.6–82.6	260–420/79.7–0.12	46.0
PMMA-H <sub>2</sub> O <sub>2</sub> MCs	122.7	95–195/98.7–81.0	210–420/80.4–0.21	36.5

conclude that the effect of viral shedding is superior for concentrations higher than  $c_1$ . At concentrations 25 and 50 mg/cm<sup>2</sup>, 90.2 and 79.2% viral clearances, respectively, are obtained. These results demonstrate that this microencapsulation system has a high potential of eliminating SARS-CoV-2.

To assess the stability of substrates functionalized with PMMA-H<sub>2</sub>O<sub>2</sub> MCs, SARS-CoV-2 tests using freshly prepared material versus preparations with three weeks of preparation were repeated (Figure 12). The results show no decrease in the ability of functionalized samples to eliminate the virus. It is even possible to visualize a slight increase; albeit being relevant and related to the uncertainty of the method and the heterogeneity of microcapsules.

Moreover, it is possible to observe differences in the percentage of virus elimination upon exposure to PMMA-H<sub>2</sub>O<sub>2</sub> MCs. During 1 h of exposure, in the virus exposure time test (Figure 10), the MCs loaded with H<sub>2</sub>O<sub>2</sub> eliminated about 97% of the virus. However, in the assay shown in Figure 11, 90% of viral elimination occurred in the presence of PMMA-H<sub>2</sub>O<sub>2</sub> MCs, while for these MCs final stability assay and in ~60% of viral elimination was registered (Figure 12). These differences can be justified because the results were obtained in three different trials and the method used is highly sensitive. Therefore, small variations in the number of virus copies present in the sample result in experimental variations associated with microcapsules. The protocol of exposure of samples to clinical isolates of SARS-CoV-2 is likely to be the reason for the variations observed in the results obtained.

Nevertheless, results between trials are consistent and differences between conditions are clear.

#### 4. CONCLUSIONS

The appearance of the SARS-CoV-2 virus continues to be a public health problem and the available disinfectants are effective for a short period of time. The goal of this work was to apply and test microcapsules loaded with H<sub>2</sub>O<sub>2</sub> on nonwoven fabrics to evaluate the efficiency to eliminate the SARS-CoV-2 virus through nucleic acid degradation. The microcapsules were characterized by SEM, TGA, and ATR-FTIR. SEM observations showed that, despite the heterogeneity in the size of microcapsules, these materials presented characteristics that make them suitable for use in disinfectant products. The regular spherical structure and absence of pores, low aggregation, and size of MCs enhanced their applicability in aqueous and solid matrices. Moreover, it was concluded that microcapsules were successfully impregnated into nonwoven fabrics. TGA showed that PMMA microcapsules loaded with H<sub>2</sub>O<sub>2</sub> had high thermal stability, delaying the decomposition of H<sub>2</sub>O<sub>2</sub>, which was a very volatile and reactive compound with oxygen. ATR-FTIR results allowed to confirm the chemical structure of PMMA MCs unloaded and loaded with H<sub>2</sub>O<sub>2</sub>. However, it was not appropriate for characterizing the microencapsulation process since no changes in molecular structure were observed in the ATR-FTIR spectrum.

The results obtained by a highly sensitive and specific RT-qPCR-based detection method to evaluate its efficacy in SARS-CoV-2 elimination strongly reinforce the functionalization of

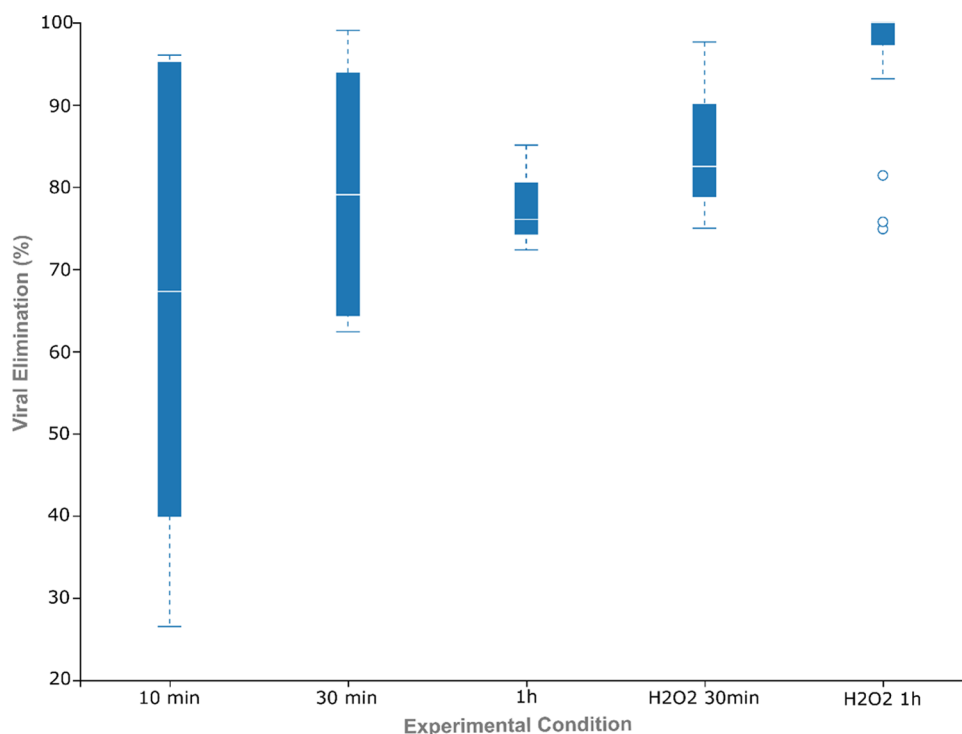


**Figure 10.** Percentage of viral SARS-CoV-2 elimination of nasopharyngeal human samples after exposure to nonfabric substrates functionalized with empty PMMA-based microparticles or PMMA microparticles containing  $\text{H}_2\text{O}_2$  at different exposure times (10 min or 1 h). Viral elimination was calculated considering the differential  $C_q$  values of treated vs nontreated samples obtained from the RT-qPCR SARS-CoV-2 nucleic acid detection method. The box plot shows a quantitative distribution of the data (10 min,  $n = 6$ ; 30 min,  $n = 6$ ; 1 h,  $n = 3$ ;  $\text{H}_2\text{O}_2$  30 min,  $n = 3$ ;  $\text{H}_2\text{O}_2$  1 h,  $n = 15$ ).

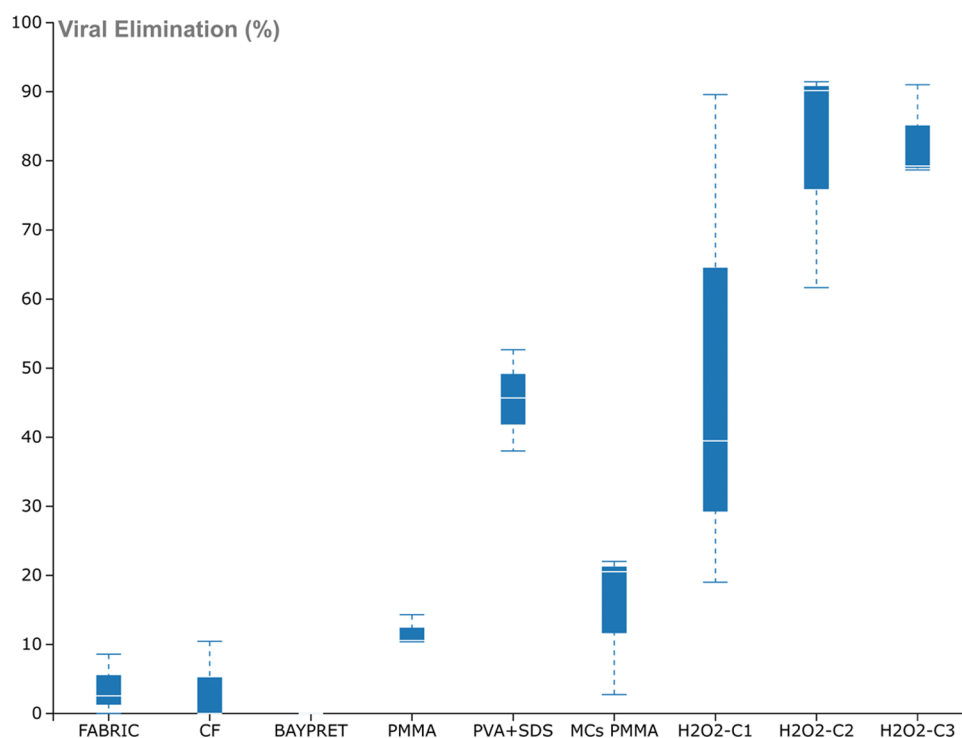


**Figure 11.** Percentage of viral SARS-CoV-2 elimination of nasopharyngeal human samples after exposure to nonfabric substrates functionalized with tissue, chloroform, BAYPRET NANO-PU, PMMA, PVA-SDS, empty PMMA-based microcapsules, and PMMA microcapsules containing  $\text{H}_2\text{O}_2$  at different concentrations ( $c_1$ ,  $c_2$ ,  $c_3$ ) during 1 h of exposure. Viral elimination was calculated considering the differential  $C_q$  values of treated vs nontreated samples obtained from the RT-qPCR SARS-CoV-2 nucleic acid detection method. The box plot shows a quantitative distribution of the data.

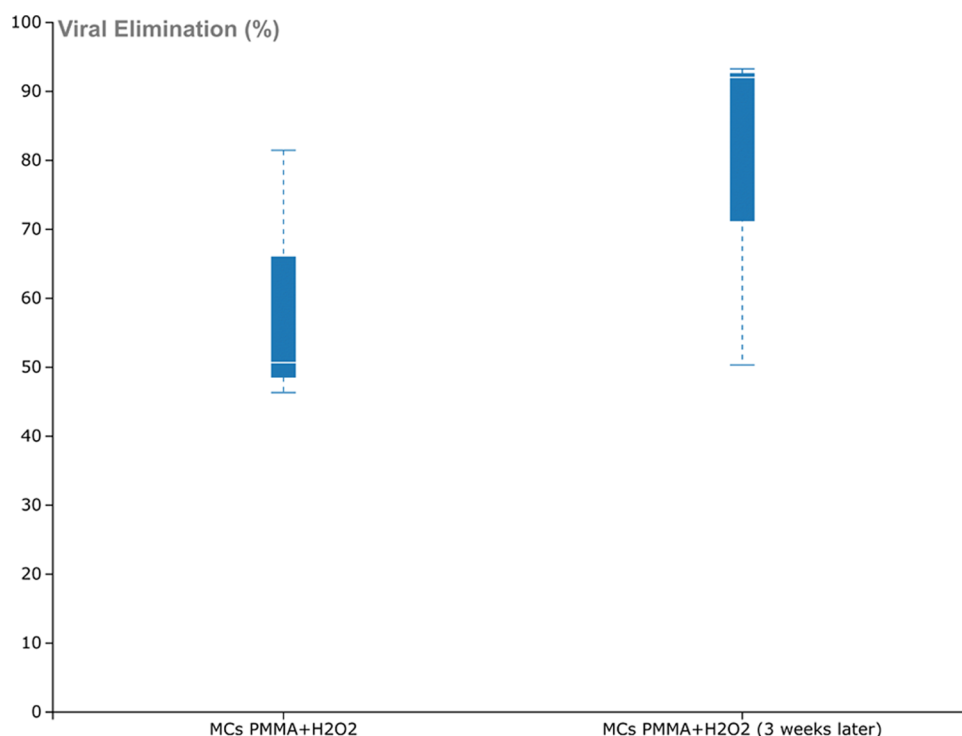


**Figure 12.** Percentage of viral SARS-CoV-2 elimination of nasopharyngeal human samples after exposure to mask tissue functionalized with freshly prepared and 3-week-old mask tissue functionalized with PMMA microparticles containing hydrogen peroxide ( $\text{H}_2\text{O}_2$ ) during 1 h of exposure. The box plot shows a quantitative distribution of the data.

fabric with PMMA MCs loaded with  $\text{H}_2\text{O}_2$  has a high potential to promote the elimination of SARS-CoV-2 contamination. The elimination of the virus in fabric samples functionalized with these MCs was above 95% after 1 h of exposure. This suggests that the method herein described could be very useful in the future development of materials that are safe and efficient in controlling the transmission of this virus. In addition, stability tests demonstrate that the functionalized samples maintain the ability to eliminate the virus with the time elapsed after the MC preparation. Virus elimination was highly dependent on the presence of PMMA- $\text{H}_2\text{O}_2$  MCs due to the low effect of the several components present in microcapsule formulation on virus elimination when separately tested.

The encapsulation avoids the rapid evaporation and degradation of  $\text{H}_2\text{O}_2$ . Some future work on the micro-encapsulation of other disinfecting agents of a similar chemical nature can easily be carried out to enhance the elimination of the virus and build a very effective disinfectant product. Thus, future developments to increase the stability of the MC formulations are of relevance to future applications.

Another topic that is quite important is the quantification of an encapsulated disinfecting agent. This subject is being developed through the construction of an analytical method with a low detection limit that allows the quantification of low concentrations of encapsulated  $\text{H}_2\text{O}_2$ . Although the quantification of  $\text{H}_2\text{O}_2$  has been extensively explored over the last few decades, the quantification of very low concentrations of  $\text{H}_2\text{O}_2$  and the disintegration of PMMA MCs without  $\text{H}_2\text{O}_2$  decomposition are still challenging topics.

However, this first preliminary study was able to demonstrate the ability of MCs PMMA- $\text{H}_2\text{O}_2$  to eliminate the SARS-CoV-2 virus in a nonwoven tissue matrix over a

period of three weeks. This prolonged effect is innovative and extremely important for an increase in disinfection time for the development of new product formulations.

## AUTHOR INFORMATION

### Corresponding Author

Carlos J. Tavares – Centre of Physics of the Universities of Minho and Porto (CF-UM-PT), University of Minho, 4835-386 Guimarães, Portugal; [orcid.org/0000-0001-5757-0096](https://orcid.org/0000-0001-5757-0096); Email: [ctavares@fisica.uminho.pt](mailto:ctavares@fisica.uminho.pt)

### Authors

Vânia I. Sousa – Centre of Physics of the Universities of Minho and Porto (CF-UM-PT), University of Minho, 4835-386 Guimarães, Portugal

Joana F. Parente – Centre of Physics of the Universities of Minho and Porto (CF-UM-PT), University of Minho, 4835-386 Guimarães, Portugal

Juliana F. Marques – Centre of Physics of the Universities of Minho and Porto (CF-UM-PT), University of Minho, 4835-386 Guimarães, Portugal; Interhigiene - Indústria De Produtos De Higiene Lda., Rua General Humberto Delgado, 4765-546 Guimarães, Portugal

Carla Calçada – Life and Health Sciences Research Institute (ICVS), School of Medicine, University of Minho, 4710-057 Braga, Portugal; ICVS/3B's—PT Government Associate Laboratory, 4806-909 Guimarães, Portugal

Maria I. Veiga – Life and Health Sciences Research Institute (ICVS), School of Medicine, University of Minho, 4710-057 Braga, Portugal; ICVS/3B's—PT Government Associate Laboratory, 4806-909 Guimarães, Portugal

Nuno S. Osório – Life and Health Sciences Research Institute (ICVS), School of Medicine, University of Minho, 4710-057

Braga, Portugal; ICVS/3B's—PT Government Associate Laboratory, 4806-909 Guimarães, Portugal

Complete contact information is available at:  
<https://pubs.acs.org/10.1021/acsomega.2c01446>

## Notes

The authors declare no competing financial interest.

## ACKNOWLEDGMENTS

The authors acknowledge the support from the project MC4COVID—Microcapsule systems for the coronavirus inactivation, funded by the Portuguese Agency IAPMEI—AGÊNCIA PARA A COMPETITIVIDADE E INOVAÇÃO, I.P., by the Foundation for Science and Technology (FCT)—project UIDB/50026/2020 and UIDP/50026/2020 and contract funding [2020.03113.CEECIND] to M.I.V. By the project NORTE-01-0145-FEDER-000039, NORTE-01-0145-FEDER-072555, and FEDER, P2020—COVID-19, reference no. NORTE-01-02B7-FEDER-069944, supported by Norte Portugal Regional Operational Programme (NORTE 2020), under the PORTUGAL 2020 Partnership Agreement, through the European Regional Development Fund (ERDF).

## REFERENCES

- (1) Tan, C.; Gao, C.; Zhou, Q.; Van Driel, W.; Ye, H.; Zhang, G. The inactivation mechanism of chemical disinfection against SARS-CoV-2: From MD and DFT perspectives. *RSC Adv.* **2020**, *10*, 40480–40488.
- (2) Ritchie, H.; Mathieu, E.; Rodés-Guirao, L.; Appel, C.; Giattino, C.; Ortiz-Ospina, E.; Hasell, J.; MacDonald, B.; Beltekian, D.; Roser, M. Coronavirus Pandemic (COVID-19) – the data *Our World in Data*, 2020 <https://ourworldindata.org/coronavirus-data>.
- (3) Chauhan, S. Comprehensive review of coronavirus disease 2019 (COVID-19). *Biomed. J.* **2020**, *43*, 334–340.
- (4) Hassan, S. A.; Sheikh, F. N.; Jamal, S.; Ezeh, Akhtar, A. Coronavirus (COVID-19): A Review of Clinical Features, Diagnosis, and Treatment. *Cureus* **2020**, *12*, No. e7355.
- (5) Singhal, T. A Review of coronavirus disease-2019 (COVID-19). *Indian J. Pediatr.* **2020**, *87*, 281–286.
- (6) Harapan, H.; Itoh, N.; Yufika, A.; Winardi, W.; Keam, S.; Te, H.; Megawati, D.; Hayati, Z.; Wagner, A. L.; Mudatsir, M. Coronavirus disease 2019 (COVID-19): A literature review. *J. Infect. Public Health* **2020**, *13*, 667–673.
- (7) Vella, F.; Senia, P.; Ceccarelli, M.; Vitale, E.; Maltezou, H.; Taibi, R.; Lleshi, A.; Rullo, E. V.; Pellicano, G. F.; Rapisarda, V.; Nunnari, Ledda, C. Transmission mode associated with coronavirus disease 2019: A review. *Health* **2020**, *24*, 7889–7904.
- (8) Wiersinga, W. J.; Rhodes, A.; Cheng, A. C.; Peacock, S. J.; Prescott, H. C. Pathophysiology, Transmission, Diagnosis, and Treatment of Coronavirus Disease 2019 (COVID-19): A Review. *JAMA* **2020**, *324*, 782–793.
- (9) Suman, R.; Javaid, M.; Haleem, A.; Vaishya, R.; Bahl, S.; Nandan, D. Sustainability of Coronavirus on Different Surfaces. *J. Clin. Exp. Hepatol.* **2020**, *10*, 386–390.
- (10) Carraturo, F.; Del Giudice, C.; Morelli, M.; Cerullo, V.; Libralato, G.; Galdiero, E.; Guida, M. Persistence of SARS-CoV-2 in the environment and COVID-19 transmission risk from environmental matrices and surfaces. *Environ. Pollut.* **2020**, *265*, No. 115010.
- (11) Chen, T. Reducing COVID-19 Transmission Through Cleaning and Disinfecting Household Surfaces Appropriate use of cleaners, sanitizers, and disinfectants against SARS-CoV-2 *Natl. Collab. Cent. Environ. Health*, 2020, p 1.
- (12) McCoy, M. How encapsulation is taking root in the laundry room. *Chem. Eng. News* **2018**, *96*, 18–22. <https://cen.acs.org/magazine/96/09605.html>
- (13) McDonnell, G. The Use of Hydrogen Peroxide for Disinfection and Sterilization Applications. In *PATAI's Chemistry of Functional Groups*; John Wiley & Sons, 2014 DOI: 10.1002/9780470682531.pat0885.
- (14) Abd Manaf, M.; Jai, J.; Raslan, R.; Subuki, I.; Mustapa, A. N. Microencapsulation Methods of Volatile Essential Oils - A Review. *Adv. Mater. Res.* **2015**, *1113*, 679–683.
- (15) Abdul Aziz, F. R.; Jai, J.; Raslan, R.; Subuki, I. Microencapsulation of Essential Oils Application in Textile: A Review. *Adv. Mater. Res.* **2015**, *1113*, 346–351.
- (16) Vishwakarma, G. S.; Gautam, N.; Babu, J. N.; Mittal, S.; Jaitak, V. Polymeric Encapsulates of Essential Oils and Their Constituents: A Review of Preparation Techniques, Characterization, and Sustainable Release Mechanisms. *Polym. Rev.* **2016**, *56*, 668–701.
- (17) Bakry, A. M.; Abbas, S.; Ali, B.; Majeed, H.; Abouelwafa, M. Y.; Mousa, A.; Liang, L. Microencapsulation of Oils: A Comprehensive Review of Benefits, Techniques, and Applications. *Compr. Rev. Food Sci. Food Saf.* **2016**, *15*, 143–182.
- (18) Atkin, R.; Davies, P.; Hardy, J.; Vincent, B. Preparation of aqueous core/polymer shell microcapsules by internal phase separation. *Macromolecules* **2004**, *37*, 7979–7985.
- (19) de Meirelles Kalil, E.; da Costa, A. J. Da Desinfecção e esterilização. *Acta Ortop Bras* **1994**, *2*, 1.
- (20) Rowan, N. J.; Meade, E.; Garvey, M. Efficacy of frontline chemical biocides and disinfection approaches for inactivating SARS-CoV-2 variants of concern that cause coronavirus disease with the emergence of opportunities for green eco-solutions. *Curr. Opin. Environ. Sci. Health* **2021**, *23*, No. 100290.
- (21) Stefanescu, E. A.; Stefanescu, C.; Negulescu, I. I. Biodegradable polymeric capsules obtained via room temperature spray drying: Preparation and characterization. *J. Biomater. Appl.* **2011**, *25*, 825–849.
- (22) Ng, S. M.; Choi, J. Y.; Han, H. S.; Huh, J. S.; Lim, J. O. Novel microencapsulation of potential drugs with low molecular weight and high hydrophilicity: Hydrogen peroxide as a candidate compound. *Int. J. Pharm.* **2010**, *384*, 120–127.
- (23) Mallepally, R. R.; Parrish, C. C.; Mc Hugh, M. A. M.; Ward, K. R. Hydrogen peroxide filled poly(methyl methacrylate) microcapsules: Potential oxygen delivery materials. *Int. J. Pharm.* **2014**, *475*, 130–137.
- (24) Mejía Suaza, M. L.; Escobar Mora, N. J.; Galeano Upegui, B. J.; Hoyos Palacio, L. M.; Cuesta Castro, D. P.; Ortiz Trujillo, I. C.; Botero Palacio, L. E.; Zapata Giraldo, J. Properties of Antibacterial Nano Textile for Use in Hospital Environments. *Rev. Ing. Bioméd.* **2017**, *11*, 13–19.
- (25) Carvalho-Correia, E.; Calçada, C.; Branca, F.; Estévez-Gómez, N.; De Chiara, L.; Varela, N.; Gallego-García, P.; Posada, D.; Sousa, H.; Sousa, J.; Veiga, M. I.; Osório, N. S. OmniSARS2: A Highly Sensitive and Specific RT-qPCR-Based COVID-19 Diagnostic Method Designed to Withstand SARS-CoV-2 Lineage Evolution. *Biomedicines* **2021**, *9*, No. 1314.
- (26) Padrão, J.; Nicolau, T.; Felgueiras, H. P.; Calçada, C.; Veiga, M. I.; Osório, N. S.; Martins, M. S.; Dourado, N.; Taveira-Gomes, A.; Taveira-gomes, A.; Ferreira, F. Development of an Ultraviolet-C Irradiation Room in a Public Portuguese Hospital for Safe Re-Utilization of Personal Protective Respirators. *Int. J. Environ. Res. Public Health* **2022**, *19*, No. 4854.
- (27) Dridi, D.; Bouaziz, A.; Gargoubi, S.; Zouari, A.; B'chir, F.; Bartegi, A.; Majdoub, H.; Boudokhane, C. Enhanced Antibacterial Efficiency of Cellulosic Fibers: Microencapsulation and Green Grafting Strategies. *Coatings* **2021**, *11*, No. 980.
- (28) Kerr, T. J.; Duncan, K. L.; Myers, L. Application of vibrational spectroscopy techniques for material identification from fire debris. *Vib. Spectrosc.* **2013**, *68*, 225–235.
- (29) JIA, X. L.; Hou, C.; Ton, Y.; Wang, J.; Ye, B. Fabrication and characterization of PMMA/HMX-based microcapsules via in situ polymerization. *Cent. Eur. J. Energ. Mater.* **2017**, *14*, 559–572.
- (30) Navarchian, A. H.; Najafipour, N.; Ahangaran, F. Surface-modified poly(methyl methacrylate) microcapsules containing linseed

oil for application in self-healing epoxy-based coatings. *Prog. Org. Coat.* **2019**, *132*, 288–297.

(31) Sarı, A.; Alkan, C.; Karaipekli, A. Preparation, characterization and thermal properties of PMMA/n-heptadecane microcapsules as novel solid-liquid microPCM for thermal energy storage. *Appl. Energy* **2010**, *87*, 1529–1534.

(32) Alsaad, A. M.; Ahmad, A. A.; Qattan, I. A.; El-Ali, A. R.; Al Fawares, S. A.; Al-Bataineh, Q. M. Synthesis of optically tunable and thermally stable pmma–pva/cuo nps hybrid nanocomposite thin films. *Polymers* **2021**, *13*, No. 1715.

(33) António, N. N. Study of the Mechanisms of Thermal Despolymerization of the Poli(methylmethacrylate). In *Dissertation for Obtaining the Master's Degree in Chemical Engineering*; Universidade Técnica de Lisboa, 2007.

(34) Hirata, T.; Kashiwagi, T.; Brown, J. E. Thermal and Oxidative Degradation of Poly(methyl methacrylate): Weight Loss. *Macromolecules* **1985**, *18*, 1410–1418.